Proceedings of the Institution of Civil Engineers
Engineering and Computational Mechanics 161
June 2008 Issue EM2
Pages 77–84
doi: 10.1680/eacm.2008.161.2.77

Paper 800010
Received 20/02/2008
Accepted 04/06/2008

Keywords: bridges/concrete structures/seismic engineering

Won K. Lee
Engineer, Forell/Elsesser Engineers, Inc., San Francisco, CA, USA

Sarah L. Billington
Associate Professor, Stanford University, Stanford, CA, USA

ice
Institution of Civil Engineers

Simulation of self-centring fibre-reinforced concrete columns

W. K. Lee PhD, MASCE and S. L. Billington PhD, MASCE

A self-centring, segmentally precast concrete column system is considered for bridges in highly seismic regions to mitigate the problem of residual displacements. Residual displacements in bridge columns can occur following severe earthquakes, and are a key indicator of post-earthquake functionality. The column system makes use of unbonded, post-tensioned steel tendons to provide self-centring to the columns, and incorporates a ductile, fibre-reinforced, cement-based composite to dissipate hysteretic energy and improve the damage tolerance of the columns. Large-scale experiments on the column system were conducted under cyclic loading, and are simulated using finite-element analysis. The goal of the simulations is to validate the ability of the finite-element models to capture the cyclic response of the columns with respect to global structural response (lateral load against displacement response) and the evolution of damage and failure modes of the columns. The models are found to perform well. The models are then used to assess column behaviour when changes are made to the ductile, fibre-reinforced material's mechanical properties, and to evaluate possible benefits that can be achieved.

NOTATION

σ_{t0} First cracking stress
ε_{t0} Strain at first cracking
σ_{tp} Peak tensile stress
ε_{tp} Strain at peak tensile stress
ε_{tu} Ultimate tensile strain
σ_{cp} Peak compressive stress
ε_{cp} Strain at peak compressive stress
ε_{cp} Ultimate compressive strain

1. INTRODUCTION

Standard highway bridges situated in highly seismic regions such as California are typically designed so that plastic behaviour will concentrate in the columns during earthquakes. The columns are expected to undergo large inelastic deformations during severe earthquakes, which can result in permanent, or residual, displacements. These residual displacements are an important measure of post-earthquake functionality in bridges, and can determine whether or not a bridge will remain usable following an earthquake. For example, following the 1995 Kobe earthquake in Japan, over 100 reinforced concrete columns with a residual drift ratio (displacement normalised by column height) of over 1·75% were demolished even though they did not collapse.[1] Residual displacements can also lead to misalignment of the superstructure, making repair and use of the bridge expensive and difficult, or not feasible. As the earthquake engineering community focuses more on performance-based design,[2] in which the post-earthquake condition of the structure is explicitly considered, engineers are beginning to take on the goal of providing post-earthquake functionality to key structures that must remain operational following an earthquake, in addition to the traditional goal of ensuring life safety (i.e. collapse prevention). Post-earthquake functionality is particularly important for highway bridges that serve as critical links in the transportation network. These links must remain unbroken to provide emergency services following an earthquake.

With increased awareness of the importance of residual displacements in highway bridge structures, and in the columns in particular, novel systems are being investigated with the goal of mitigating the effects of residual displacements. The primary method of dealing with large, expected inelastic deformations is to provide a restoring force to bring the structure back to its original position: that is, to provide self-centring to the structure. Several systems have recently been investigated for bridge systems,[3–5] and one such system is shown in Fig. 1.[6] In this system the columns consist of precast concrete segments for ease of construction and improved durability. Each individual segment contains bonded steel reinforcement, but there is no bonded reinforcement crossing the joints between the segments. Unbonded, post-tensioned (UBPT) steel tendons are used as the primary, continuous longitudinal reinforcement through the columns.

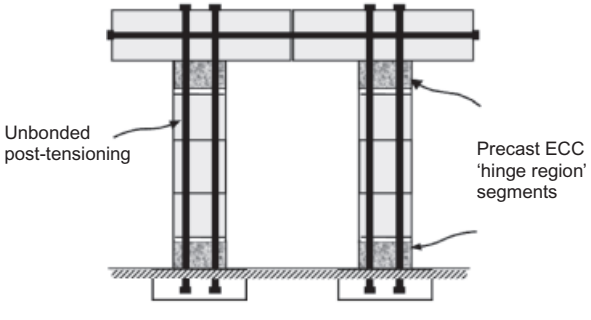

Fig. 1. Self-centring system bridge piers using unbonded post-tensioning to provide restoring force

The fact that the post-tensioning tendons are unbonded rather than bonded means that strains in the member will not localise in the tendons at cracking locations; strains in the concrete will still vary along the length of the member, and are expected to localise at the member ends. The even distribution of member strains to the entire length of the tendons leads to significantly lower strains in the tendons, and the member can be designed so that the tendons will remain elastic even under conditions approaching failure. Therefore the UBPT tendons supply a restoring force ('self-centring') to the columns.

Although the UBPT provides self-centring to the system, laterally loaded columns sustain physical damage, manifested by spalling of concrete cover and localised cracking. To provide improved resistance to this type of damage, the proposed system incorporates a ductile, fibre-reinforced cement-based composite material, known as engineered cementitious composite (ECC). ECC typically contains Portland cement, water, fine sand, fly ash, and roughly 2% or less by volume of high-aspect ratio (typically polymeric) fibres. ECC is so called because its mechanical properties can be tailored through careful selection of the mix proportions to provide the desired response.[7]

ECCs typically have high tensile strain capacities, and exhibit strain-hardening-like behaviour after cracking, up to strains of 3%. They are also self-confining to some extent, and do not spall in compression.[8] Compressive strengths comparable to or greater than those of commonly used 'normal-strength' concretes (28–42 MPa) are typically targeted for ECC. Due to the lack of coarse aggregate, the elastic modulus of ECC is generally lower than that of ordinary concrete, but the compressive strength is similar. In addition, the creep response of ECC is generally greater than that of ordinary concrete,[9] which can result in greater prestressing losses in the UBPT tendons. However, such additional prestressing losses can be accounted for in the design of the initial prestressing force.

Both the tensile and the compressive features of ECC are expected to provide improvements to the damage tolerance of the columns. Due to the greater cost of ECC compared with ordinary concrete, it is proposed for application in the regions of the column where its use would be most beneficial. For columns subjected to double curvature under lateral loading, as shown in Fig. 1, these are the ends of the columns, where the moments are the highest.

The objective of this study is to assess the ability of finite-element modelling methods to predict the overall behaviour of the UBPT column system, in terms both of global lateral load–displacement behaviour and of local damage response. Validation of such analytical tools in predicting the response of new structural systems is especially important in earthquake engineering, which relies heavily on simulations to assess structural response under seismic loadings. In addition, the finite-element models are used to assess the impact on the system, and the possible benefits, of modifying the mechanical properties of the ECC.

2. BACKGROUND TO EXPERIMENTS

The experimental programme comprised the testing of a set of six, large-scale UBPT bridge columns. Full details of the experiments are given by Rouse.[10] The column specimens were 3·7 m high and 460 mm by 460 mm in cross-section. The specimens consisted of precast segments with cap and foundation blocks. Each column comprised four precast segments, each 1·067 m long, with the two end segments embedded in the cap and foundation blocks. The precast segments were connected with a flowable epoxy mortar, and had no continuous bonded reinforcing across the segmental joints. The segments were post-tensioned together with six low-relaxation strands, 15·2 mm in diameter, stressed to 690 MPa.

The specimens were tested in double curvature in order to represent the behaviour of a column in a multiple-column bent configuration subjected to lateral loading. To achieve this deformation behaviour two specimens were tested simultaneously, as shown in Fig. 2. Specimens were oriented horizontally (longitudinal axis parallel to the floor), with their foundation blocks connected to a steel reaction frame and their cap blocks connected to one another to provide rotational restraint. The specimens were subjected to quasi-static cyclic lateral loads while under a constant axial load of 720 kN (applied with a hydraulic actuator), representing the dead load from a bridge superstructure. This load corresponded to an axial load ratio of approximately 8·5%.

One of the variables in the experiments was the material in the two end segments of the column, referred to herein as the hinge segments. These are the segments in which plastic behaviour is expected to concentrate, and hence are those in which the greatest damage is expected to occur under severe lateral loading. The three hinge segment materials considered were concrete and two types of ECC. Again, the ECC was expected to provide improvements to the response of the column as compared with ordinary concrete. The first ECC (ECC-1) used polyethylene fibres with ultra-high molecular weight, and the second one (ECC-2) used polyvinyl alcohol fibres. Both types of ECC contained fibres at a volume fraction of 2% and had compressive strengths of the order of 35–45 MPa. Typical uniaxial tensile stress–strain curves for the two types of ECC, obtained from tension tests, are shown in Fig. 3. Experimental and simulation results from the specimen with ECC-1 are presented here. The properties of ECC-2 are considered analytically here when evaluating the impact of changing ECC properties on column system response.

Lightweight concrete was used for the remaining segments (including cap and foundation blocks), with a nominal compressive strength of 55 MPa at the time of testing, as determined by cylinder tests. The reinforcement in the column segments was detailed to meet only the shear and shrinkage requirements of the 1996 American Association of State and Highway Transportation Officials (AASHTO) standard specifications.[11] Reinforcement details of the column segments can be seen in Fig. 4.

3. FINITE-ELEMENT MODEL

A plane stress model was used in the analyses, as out-of-plane stresses were assumed to be negligible for the testing configuration. Each column was modelled individually. The finite-element model for a single column is shown in Fig. 5. The concrete and ECC were modelled using nine-noded,

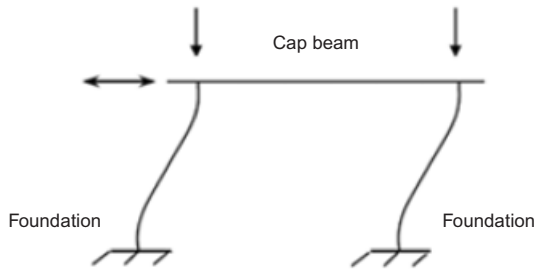

Multiple pier bent, elevation view

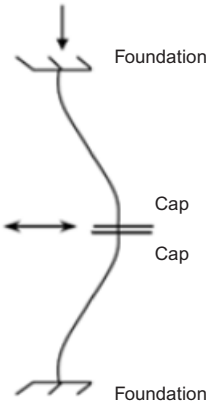

Test set-up, plan view

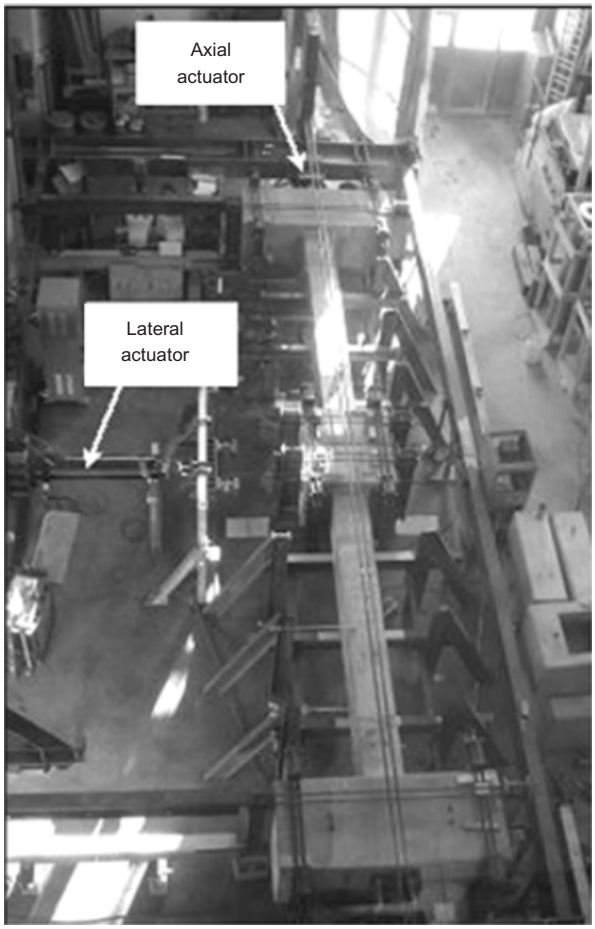

Fig. 2. Experimental set-up of UBPT column tests

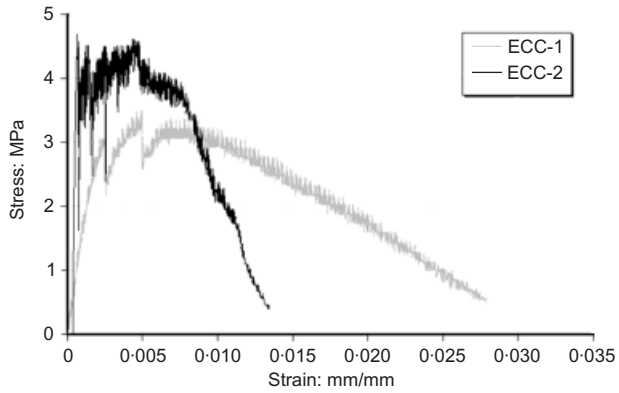

Fig. 3. Typical uniaxial tensile stress–strain behaviour of ECC mixes

quadrilateral isoparametric plane stress elements with a 3×3 Gauss integration scheme. All longitudinal- and transverse-bonded mild steel reinforcing bars were modelled with three-noded embedded reinforcement elements, which were assumed to have a perfect bond with the surrounding plane stress elements. The bonded longitudinal reinforcing bars in the column segments did not have adequate development length to reach their yield strength in all areas. Where reinforcing bars did not have adequate development, the yield stress of the elements constituting the reinforcing bar was reduced in a step-wise fashion from 100% of the yield stress at the point of full development to zero at the end of the bar in order to approximate the linear reduction in bond stress. The development length for the bars was computed according to Lowes *et al.*[12] Full details of the reinforcing bar modelling can be found in Lee.[13]

The UBPT tendons were modelled with two-noded truss elements that were constrained at their end nodes to the concrete element nodes at the anchorage locations. This connectivity allowed the strains to be distributed evenly along the length of the post-tensioned tendons. An initial stress of 690 MPa, equal to the experimental prestress in the tendons, was applied to the truss elements. Cracking at the unreinforced joint regions was represented by smeared cracking in the plane stress elements. Interface elements are often used to model discrete cracks when the location of cracking is known a priori, for example at a known plane of weakness. In the case of the columns modelled here the precast column segments were connected using an epoxy mortar with a tensile strength (63 MPa at 14 days, as reported by the manufacturer) greater than that of the segments themselves. Therefore cracking was not expected to occur in the mortar between the segments, and thus the joints between segments were not explicitly modelled using interface elements.

The foundation block was modelled as fixed by providing pin supports at all nodes along the bottom of the model. The top

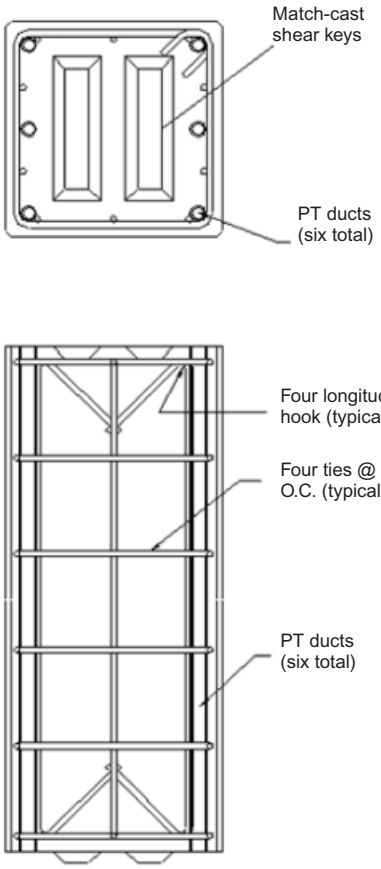

Fig. 4. Column segment reinforcement details

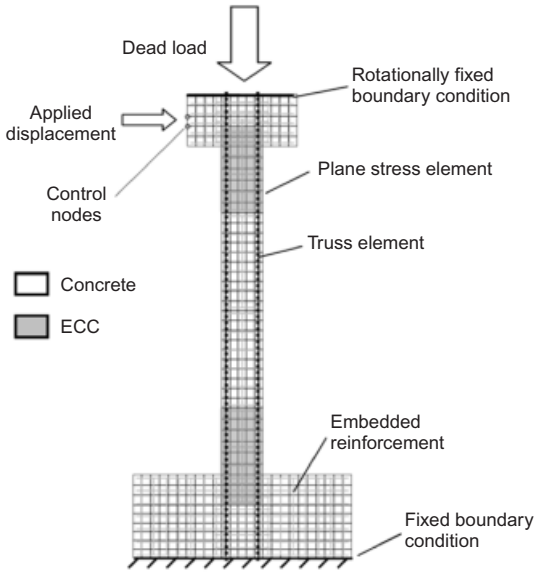

Fig. 5. Finite-element model for UBPT column specimen

nodes of the specimen (at the top of the cap block) were modelled as being rotationally fixed to represent the fixity provided by the connection to the cap of the other specimen. Because rotational degrees of freedom do not exist for the quadrilateral elements, rigid three-noded beam elements were added along the top of the cap, and their rotational degrees of freedom were constrained to provide the appropriate fixity. Point loads with a total magnitude equal to the magnitude of the applied axial load were applied to the top nodes of the cap block. Lateral loading was applied through applied displacements at two control nodes in the cap. Geometric non-linearity was included in the analyses in addition to material non-linearity.

4. CONSTITUTIVE MODELS

The concrete elements in the footing and the cap were modelled as linear elastic, because non-linear behaviour in those regions (as manifested by cracking or crushing) was neither expected nor observed during testing. The elastic modulus of the concrete was not measured in the experiments by Rouse:[10] therefore the elastic modulus for the concrete in these and all other concrete segments was assumed to be 24·8 GPa, based on the American Concrete Institute (ACI) 318 equation[14] for lightweight concrete using measured compressive strength data.

To model the tensile behaviour of concrete, a smeared rotating crack model with a total strain formulation was used.[15] The model is based on the equivalent uniaxial strain concept. The cracking behaviour was assumed to be linear until first cracking, with a stiffness equal to the compressive modulus (24·8 GPa). The post-cracking behaviour was defined to be fracture energy based with linear tension softening. The tensile strength was assumed to be 3·45 MPa, as computed from the ACI 318 equation[14] for modulus of rupture of lightweight concrete. The tensile fracture energy was assumed to be 0·4 N mm/mm^2 as calculated from the CEB-FIP model code.[16]

A bilinear model was used for the bonded, mild steel reinforcing. The assumed yield strength for the bonded reinforcing steel was 460 MPa (66·8 ksi), which is a mean value of yield strength for Grade 60 steel.[17] The elastic modulus was set as 200 GPa, and the post-yield (hardening) slope was assumed to be 2% of the elastic modulus. The UBPT tendons were modelled as linear elastic, as designed and as observed throughout the testing, with an elastic modulus of 186 GPa.

The ECC was modelled with a total strain-based, rotating crack model developed by Han *et al.*[18] This model is based on the observed responses from a series of reversed cyclic tests on uniaxially loaded ECC specimens,[18] and was validated against cyclically loaded components. The envelope curves are shown in Fig. 6. The unloading and reloading paths of the constitutive model were developed to capture the unique cyclic behaviour

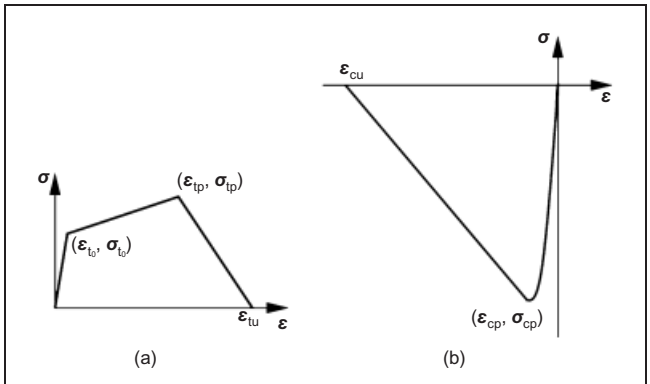

Fig. 6. Envelope curves for ECC constitutive model in (a) tension and (b) compression

of ECCs. The ECC constitutive model was modified here to incorporate non-linearity in the envelope curve in compression. The pre-peak portion of the compressive stress–strain envelope was changed from linear to a curve following the Popovics equation.[19]

The tensile stress and strain values for the envelope curve of the model were based on uniaxial tensile tests on ECC-1.[10] The peak compressive stress was based on cylinder compression tests. As the compressive stress–strain behaviour of the ECC was not measured in the experiments by Rouse,[10] the assumed elastic modulus and peak compressive strain were based on tests performed on ECCs with similar mix proportions and similar compressive strengths to those reported by Kesner *et al.*[20] The loading and unloading parameters for the constitutive model from Han *et al.*[18] were adopted here.

5. SIMULATION OF SELF-CENTRING COLUMN WITH ECC-1

Two ECC columns were tested together in the experiments by Rouse;[10] that is, with their cap blocks connected. A monotonic simulation was performed for the specimen that contained ECC-1 in the hinge segments, as it was the first of the two specimens to fail. The resulting monotonic load–drift response is shown, compared with the experimental response, in Fig. 7(a). The experimental load–drift response was corrected for measured deflections due to flexibility in the reaction frame. In the experiment, the column reached its peak strength during the cycle to approximately 2% drift. After the column had reached its strength capacity, the initial boundary conditions that deformed the specimens in double curvature were no longer being applied as intended in the experiment. Therefore the final one-and-a-half large cycles (to approximately 3% and 4% drift) cannot be directly compared with the simulated response, which maintains the initial boundary conditions.

The simulation captures the envelope curve of the response well. The peak load predicted in the simulations was 214 kN at a drift of 1·54%, whereas the peak load in the experiment was 201 kN at a drift of 1·62%. The initial stiffness of the simulation, computed at a drift of 0·15%, was 7770 kN/m, and the initial stiffness of the experiment was 7735 kN/m, a difference of less than 1%. The initial stiffness for the column is lower than that of an all-concrete column would be, because the elastic modulus of the ECC is lower than that of concrete.

The column reaches its peak lateral load soon after crack localisation occurs in the column near the joint between the end segments (made with ECC-1) and the adjacent concrete segments (as shown in Fig. 8). Although there is longitudinal, bonded mild steel reinforcement at this section, it is unable to contribute significantly to the moment capacity, because it cannot reach its yield strength owing to its development length (recall that the mild steel reinforcement is not continuous across the joints). The ECC is therefore relied on primarily to resist tensile stresses. After the ECC begins to soften in tension (crack localisation), the crack progresses towards the compression region, reducing the size of the compressive zone and causing the ECC in compression to quickly reach its peak strain and begin to soften. At this point the column begins to lose its lateral load resistance. The fact that there is no steel yielding leads to a relatively brittle and therefore undesirable failure.

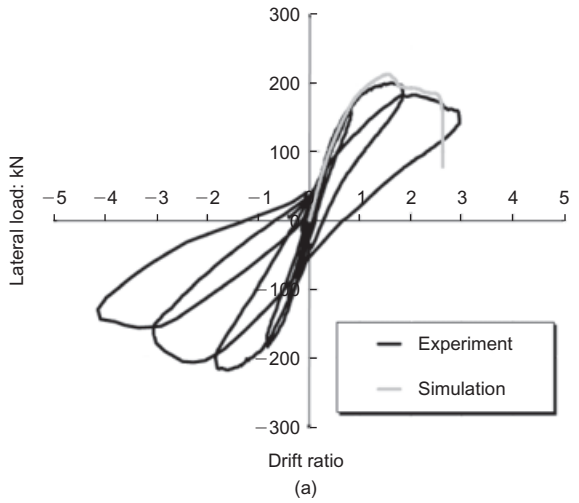

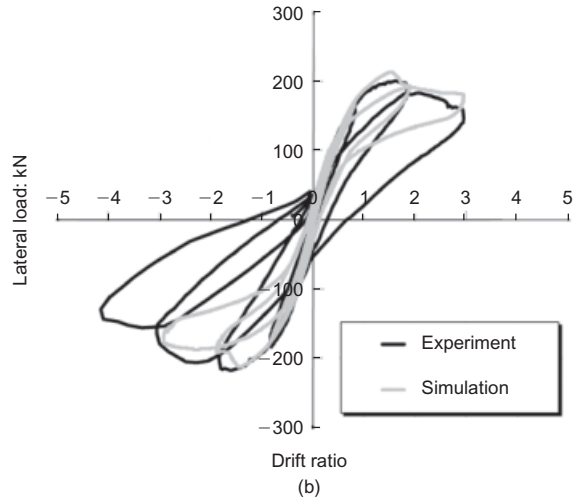

Fig. 7. Comparison of (a) monotonic and (b) cyclic analysis with experiment

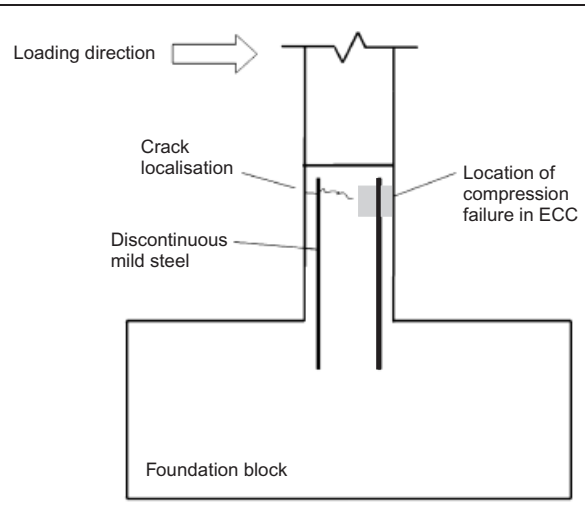

Fig. 8. Region of crack localisation and compressive strain localisation

The formation of the localised crack near the joint and the subsequent compressive failure of the ECC were both observed in the experiment. The simulation fails to converge at a drift of approximately 2·6% owing to strain-softening in the ECC in

compression (as shown in Fig. 8). The actual specimen continued to soften to 2·9% drift, when the loading direction was reversed for the final cycle.

A cyclic analysis was performed next. The results are shown in Fig. 7(b). The envelope of the simulated cyclic response generally follows the experiment well. During the lower drift cycles, low residual displacements (displacement at zero load) are seen in both the experiment and the simulation. Additionally, up to the 3% drift cycle, the simulation captures a similar peak strength and displacement as the experiment, and the observed gradual softening to 3% drift is also simulated. The downward slope to increasing drifts (e.g. from 2% to 3% drift) is indicative of *P*–delta effects due to the gravity load on the column, and is less prominent in the simulation, although geometric non-linearity is included in the simulations. At the largest drift cycle (to 3% drift) the simulated response no longer models the experimental response well, particularly in unloading. The simulated response displays the expected flag-shaped (origin-oriented) response, whereas the experimental response follows a much less stiff unloading path. The less stiff experimental unloading is caused by the change in boundary conditions in the experiment relative to the simulation (i.e. the lower stiffness of deformation in single curvature compared with double curvature). The wider hysteresis loops are attributed to the spread of ECC crushing not captured in the simulation, and to additional effects that are not modelled, such as possible slip of bonded steel reinforcement after cracks localise.

6. IMPACT OF ALTERNATIVE ECC MATERIAL DESIGN

The ECC column had a low drift capacity and a relatively brittle failure mode, both of which are unfavourable for structures in seismic regions. As ECC is an engineered material, its tensile response can be tailored to meet the requirements of the engineer. Therefore a parameter study was performed to determine the effect of the ECC tensile parameters on the load–drift behaviour of the columns. The goal of this study was to evaluate the effect of alternative ECC material designs on the structural response to show possible benefits of engineering new ECC mix designs, specifically with respect to increasing drift capacity and introducing greater ductility in the column prior to failure.

To determine the effect of the ECC tensile parameters on the global response, the model was reanalysed for three different tensile stress–strain responses, as shown in Fig. 9. The first case (model 1) assumed an increase in first cracking strength of the ECC, with no increase in ductility (i.e. the same strain at peak stress) relative to ECC-1 in the experiment. The slope of the hardening branch was kept the same. The second case (model 2) assumed an increase in ductility by maintaining the same hardening slope but allowing the hardening to occur to 1·37%, which is twice the amount of strain-hardening as in the original model. The third case (model 3) assumed strain-hardening behaviour to a higher peak strain of 3%, but maintaining the stress at peak strain of the original model (at 3·45 MPa), effectively giving the material a shallow hardening behaviour. The three models represent behaviour that can reasonably be expected from an ECC mix.[21]

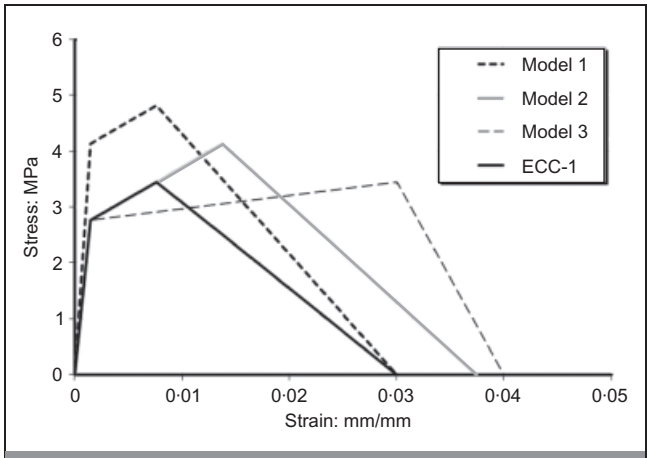

Fig. 9. Alternative models for ECC tensile envelope

The load–drift response of the column using Model 1 for the ECC, with increased cracking strength, is compared with the experimental response and the simulated response using the original ECC model (ECC-1) in Fig. 10(a). The response with increased ECC strength is similar to that of the original model, but with a 2% increase in the peak load and a 36% increase in the drift at peak load. The localisation of cracking in this case occurs in the concrete segments above the ECC segments rather than in the ECC segments themselves, because the cracking strength of the ECC exceeds the concrete cracking strength. The area of localisation in the concrete segments is shown in Fig. 11. The column fails when the compressive strength of the ECC is reached, and begins to soften soon afterwards at the segmental joint between the ECC and concrete segments, near the point of crack localisations.

The increased strength of the ECC as described by model 1 did not provide significant improvements to the overall behaviour of the column. The peak drift and lateral load were increased over the original case, but compressive failure still occurred at a relatively low drift and near the segmental joint where the mild steel reinforcement cannot be fully developed, preventing the ability to yield and hence resulting in a lack of ductility. The region of crack localisation was changed from the ECC hinge segment to the concrete segment, but this did not significantly alter the global behaviour.

The resulting load–drift response for model 2, with moderate ductility and strength increases over ECC-1, is shown in Fig. 10(b), compared with the experimental response and the simulated response using ECC-1. Again, there is an increase in the simulated peak load due to the increased ECC strength in model 2. The localisation of cracking again occurs in the concrete segments just above the segmental joint between the ECC and the concrete, but is delayed with respect to the original model. Localisation is delayed in this case because although the ECC cracks at a lower stress than the strength of the concrete, it then hardens to a peak stress higher than the strength of the concrete. The area of localisation of cracking in the concrete segment can be seen in Fig. 11. Similar to the case of model 1, the critical section is in the joint region, where the mild steel reinforcement in unable to contribute significantly to the moment capacity owing to its development length. The moderate increase in ductility described by model 2 again provides only minimal improvements to the overall behaviour of the column.

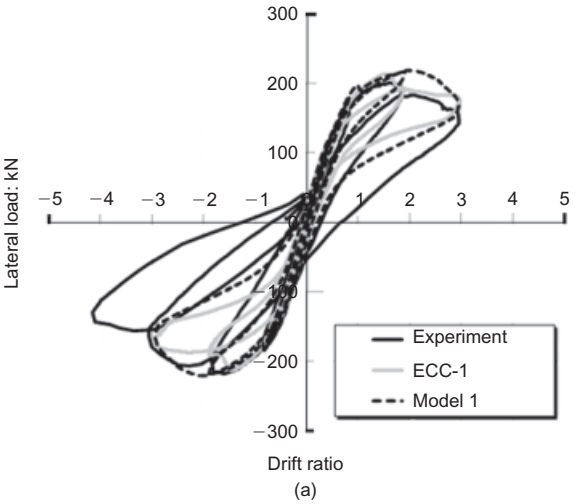

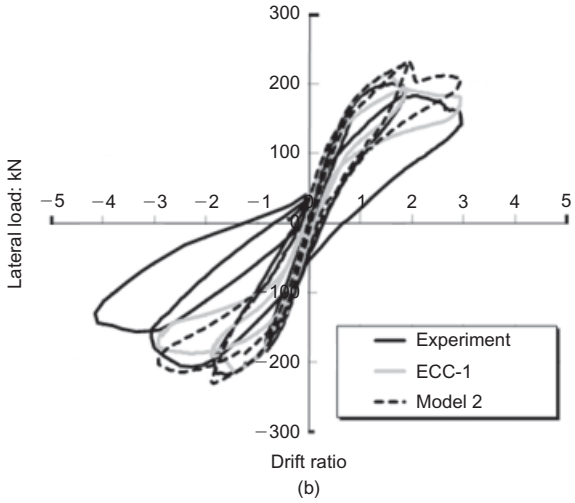

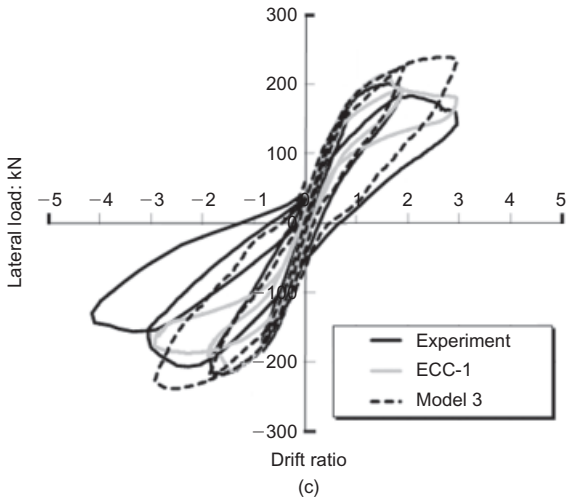

Fig. 10. Comparison of cyclic behaviour of experiment and simulation for: (a) model 1; (b) model 2; (c) model 3

The final model, model 3, provides an even greater increase in the strain-hardening capacity of the ECC in tension, but—perhaps more importantly—limits the peak strength from exceeding the tensile strength of the concrete. The resulting load–drift response for model 3 is compared with the experimental response and the simulated response using ECC-1 in Fig. 10(c). The response of the column with ECC model 3 shows a distinct difference from those of ECC-1 and models 1 and 2. By 3% drift the column continues to carry additional load (no peak is reached followed by softening). In this case the maximum tensile strains occur at the ends of the columns (column–base interface), and localisation of cracking does not occur near the segment joints between the ECC and the concrete. The area of localisation of cracking in the segment can be seen in Fig. 11. Cracking and strain-hardening of the ECC occur throughout most of the hinge segment, with the greatest tensile straining occurring at the ends. Localisation of cracking does not occur in the concrete, because the tensile strains continue to accumulate in the ECC while not reaching a strength exceeding that of the concrete. Since the localisation of cracking occurs at the base of the column, the mild steel is able to contribute more significantly to the moment capacity, because in this region it has adequate development length. The ability of the mild steel to yield provides ductility and additional moment capacity to the column, as compared with the original ECC model (ECC-1) and models 1 and 2.

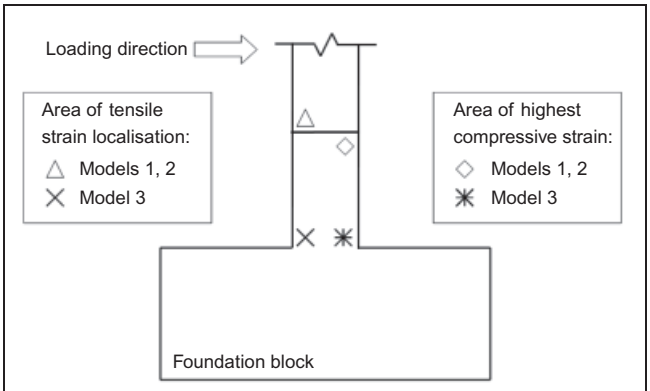

Fig. 11. Location of tensile strain localisation and compressive failure for alternative ECC models

The parameter study of the ECC tensile behaviour revealed that the best way to improve the performance of the columns is to increase the ductility of the ECC without increasing the ultimate tensile strength. Increasing the ultimate tensile strength of the ECC to a value greater than that of the tensile strength of the concrete is predicted to lead to crack localisation above the base segment (the plastic hinging region). High ECC tensile strength would lead to compressive failure near the segmental joint between the ECC and the adjacent concrete segment. Increasing the tensile ductility while keeping the peak tensile stress below the tensile strength of the concrete makes better use of the tensile benefits of the ECC. Cracking is predicted to occur throughout the ECC segment, and a crack will eventually localise at the base of the column. In addition, the failure location is shifted away from sections where mild steel reinforcement is not able to yield fully (i.e. near the joints) to sections where it can contribute more significantly to moment capacity and improve ductility (i.e. at the ends of the column).

7. CONCLUSION

A self-centring, unbonded, post-tensioned bridge column system with precast, segmental construction using ductile, fibre-reinforced, cement-based composite materials was simulated using two-dimensional non-linear finite-element analysis. The finite-element model was found to capture the

response of the column well, with respect both to global behaviour (lateral load against displacement response) and to local, damage behaviour (development of damage and mode of failure). The mode of failure of the column at a relatively low drift was captured well.

As ECC is an engineered material, and its tensile response can be tailored to meet the requirements of the structure, a parameter study was conducted to evaluate alternative ECC tensile stress–strain envelopes and their impact on column failure modes and damage response. In particular, an ECC tensile stress–strain response was sought to improve the drift capacity and prevent relatively brittle failure. The study showed that increasing the tensile strain capacity of the ECC without increasing the peak strength was predicted to be the best means of altering the ECC behaviour to achieve higher strength and ductility accompanied by damage localisation at the base of the columns, where bonded mild steel reinforcement can yield fully.

REFERENCES

1. KAWASHIMA K., MACRAE G., HOSHIKUMA J. and NAGAYA K. Residual displacement response spectrum. *ASCE Journal of Structural Engineering*, 1998, **124**, No. 5, 523–530.
2. MOEHLE J. and DEIERLEIN G. A framework methodology for performance-based earthquake engineering. *Proceedings of the 13th World Conference on Earthquake Engineering, Vancouver*, August 2004. Paper No. 679
3. SAKAI J., JEONG H. and MAHIN S. Earthquake simulator tests on the mitigation of residual displacements of reinforced concrete bridge columns. *Proceedings of the 21st US–Japan Bridge Engineering Workshop, Tsukuba, FHWA, McLean, Japan*, 2005.
4. YAMASHITA R. and SANDERS D. *Shake Table Testing and an Analytical Study of Unbonded Prestressed Hollow Concrete Columns Constructed with Precast Segments*. Center for Civil Engineering Earthquake Research, University of Nevada, Reno, 1995, Report CCEER 05-9.
5. ZATAR M. and MUTSUYOSHI H. Reduced residual displacements of partially prestressed concrete bridge piers. *Proceedings of the 12th World Conference on Earthquake Engineering, Auckland*, 2000, **2**.
6. ROUSE J. M. and BILLINGTON S. L. Behavior of bridge piers with ductile fiber reinforced hinge regions and vertical, unbonded post-tensioning. *Proceedings of the FIB Symposium on Concrete Structures in Seismic Regions*, Athens, 2003.
7. LI V. C. and LEUNG C. Steady-state and multiple cracking of short random fiber composites. *Journal of Engineering Mechanics*, 1992, **118**, No. 11, 2246–2264.
8. BILLINGTON S. and YOON J. Cyclic response of unbonded posttensioned precast columns with ductile fiber-reinforced concrete. *Journal of Bridge Engineering*, 2004, **9**, No. 4, 353–363.
9. ROUSE J. M. and BILLINGTON S. L. Creep and shrinkage of high-performance fiber-reinforced cementitious composites. *ACI Materials Journal*, 2007, **104**, No. 2, 129–136.
10. ROUSE J. M. *Behavior of Bridge Piers with Ductile Fiber Reinforced Hinge Regions and Vertical Unbonded Post-Tensioning*. PhD thesis, Cornell University, New York, 2004.
11. AASHTO. *Standard Specifications for Highway Bridges*. American Association of State and Highway and Transportation Officials, Washington, DC, 1996.
12. LOWES L. N., MITRA J. and ALTOONTASH A. *A Beam–column Joint Model for Simulating Earthquake Response of Reinforced Concrete Frames*. Pacific Earthquake Engineering Research Center, University of California, Berkeley, 2003, Report PEER 2003/10.
13. LEE W. K. *Simulation and Performance-based Earthquake Engineering Assessment of Self-centering Post-tensioned Concrete Bridge Systems*. PhD thesis, Stanford University, Palo Alto, CA, 2007.
14. AMERICAN CONCRETE INSTITUTE. *Building Code Requirements for Structural Concrete and Commentary*. ACI, Farmington Hills, MI, 2005, ACI 318-05 and ACI 318R-05.
15. FEENSTRA P. H., ROTS J. G., ARNESEN A., TEIGEN J. G. and HOISETH K. V. A 3D constitutive model for concrete based on a co-rotational concept. *Proceedings of the Euro-C Conference on Computational Modelling of Concrete Structures*, Badgastein, 1998, pp. 13–22.
16. CEB-FIP. *Bulletin d'Information*. CEB, Lausanne, 1990.
17. MELCHERS R. E. *Structural Reliability Analysis and Prediction*. Wiley, Chichester, 1999.
18. HAN T. S., FEENSTRA P. H. and BILLINGTON S. L. Simulation of highly ductile cement-based composites. *ACI Structural Journal*, 2003, **100**, No. 6, 749–757.
19. POPOVICS S. A numerical approach to the complete stress–strain curves for concrete. *Cement and Concrete Research*, 1973, **3**, No. 5, 583–599.
20. KESNER K., BILLINGTON S. L. and DOUGLAS K. S. Cyclic response of highly ductile fiber-reinforced cement-based composites. *ACI Materials Journal*, 2003, **100**, No. 5, 381–390.
21. LI V. C., MISHRA D. K. and WU H. C. Matrix design for pseudo-strain-hardening fibre reinforced cementitious composites. *RILEM Journal of Materials and Structures*, 1995, **28**, No. 183, 586–595.